

# Ultra-sensitive Photothermal Spectroscopy: Harnessing the Seebeck Effect for Attogram-Level Detection

Yaoli Zhao<sup>1</sup>, Patatri Chakraborty<sup>1</sup>, Ali Passian<sup>2</sup>, and Thomas Thundat<sup>1</sup>

<sup>1</sup>Chemical and Biological Engineering, University at Buffalo, Buffalo, NY 14260, USA

<sup>2</sup>Quantum Computing and Sensing, Oak Ridge National Laboratory, Oak Ridge TN 37831, USA

## Abstract

Molecular-level spectroscopy is crucial for sensing and imaging applications, yet detecting and quantifying minuscule quantities of chemicals remains a challenge, especially when they surface-adsorb in low numbers. Here, we introduce a photothermal spectroscopic technique that enables the sensing and quantification of adsorbates with an attogram detection limit. Our approach utilizes the Seebeck effect in a microfabricated nanoscale thermocouple junction, incorporated into the apex of a microcantilever. We observe minimal thermal mass exhibited by the sensor which maintains exceptional thermal insulation. The temperature variation driving the thermoelectric junction arises from the non-radiative decay of molecular adsorbates' vibrational states on the tip. We demonstrate the detection of physisorbed trinitrotoluene (TNT) and dimethyl methylphosphonate (DMMP) molecules, as well as representative polymers, with an estimated mass sensitivity of  $10^{-18}$  g and a temperature resolution of 40 mK.

**KEYWORDS:** *Molecular recognition, calorimetry, microfabricated thermocouple, photothermal spectroscopy, infrared sensor*

One of the most crucial attributes of a chemical sensor is its selectivity, which refers to the sensor's ability to differentiate between two chemical species with similar molecular properties<sup>1</sup>. Traditional molecular recognition methods, based on room temperature reversible adsorption on immobilized chemical interfaces (receptors) on sensor surfaces, often suffer from poor selectivity due to the generic nature of weak chemical interactions<sup>2, 3</sup>. Additionally, non-uniformity in immobilized functional coatings can lead to unacceptable sensor-to-sensor response variability<sup>4-6</sup>. The latter is even more pronounced in micro-, and nano-sensors compared to macro-sensors, such as quartz crystal microbalances (QCM), due to their smaller surface areas<sup>6, 7</sup>. The limited selectivity of miniature sensors remains a significant obstacle to their wider adoption and commercialization. As a result, enhancing the sensitivity and selectivity of these sensors has become a primary focus in the field<sup>8-12</sup>, encompassing both classical and emerging quantum sensors<sup>13-16</sup>.

Current chemical sensing methods for complex mixtures, such as sensor arrays modified with partially selective layers (e.g., electronic noses<sup>17</sup>), struggle to provide reliable results while exhibiting high sensor-to-sensor response variations<sup>18, 19</sup>. Consequently, there is a pressing need for miniature sensing mechanisms that do not rely on functional selective layers. Mechanically robust and environmentally stable sensors that depend on weak intermolecular forces (physisorption) for molecular adsorption are particularly sought after. Chemical reactions based on physisorption, or Van der Waals-type interactions are typically reversible.

In an effort to overcome the issue of insufficient chemical selectivity, studies have focused on the combination of microfabricated structures, including microcantilevers and micro-strings, with infrared (IR) spectroscopy<sup>17, 20, 21</sup>. This approach aims to enhance chemical sensors' selectivity and sensitivity by leveraging the microfabricated structures' unique properties and advantages of IR spectroscopy. Detailed information about adsorbed materials' chemical composition and molecular structure can be obtained in the mid-IR ( $\sim 400\text{-}4000\text{ cm}^{-1}$  or  $2.5\text{-}25\text{ }\mu\text{m}$ ) encompassing the characteristic absorption bands of various functional groups and bonds present in organic and inorganic compounds<sup>22</sup>. The NIR region ( $\sim 4000\text{-}12500\text{ cm}^{-1}$ , or  $800\text{-}2500\text{ nm}$ ), while having its own advantages in certain cases, is dominated by overtones and combination bands of the

fundamental vibrations, which can lead to broad, overlapping bands, making the interpretation of spectral features more challenging<sup>23-25</sup>.

Microstructures, known for their sensitive transduction of temperature variations, provide an excellent platform for photothermal and photoacoustic spectroscopy<sup>26, 27</sup>. Layered structures with differing thermal properties can undergo deformation, both when interacting directly with IR radiation and indirectly through the nonradiative decay of adsorbed molecules excited by IR radiation. For instance, bi-material cantilevers and micro-strings have been reported to generate the spectrum of the radiation source, as well as the spectra of adsorbed molecules interacting with the excitation radiation, due to the development of asymmetric stress distribution<sup>28, 29</sup>. The observed signals effectively display both the mechanical resonance spectrum of the oscillator (e.g. when the source is properly amplitude modulated) and the molecular resonance spectrum when the source is tuned spectrally. One advantage of these techniques is their receptor-free operation. However, the sensitivity relies on the thermal capacitance of the sensor, meaning higher (heat) energies are needed to increase the sensor temperature. Consequently, the technique's sensitivity is limited by the mass of the device<sup>20, 21</sup>.

The prevalent use of microcantilever probes in various scanning probe microscopy (SPM) applications and the growing interest in localized temperature measurements have spurred the development of cantilevers with nanoscale thermocouples integrated into their tip regions<sup>30, 31</sup>. For instance, in scanning thermal microscopy (SThM), these specialized probes are utilized for the thermal mapping of samples<sup>32-34</sup>. The embedded thermocouples possess low thermal capacitance, meaning they do not exhibit high heat absorption and storage. SThM cantilevers, commonly used for surface temperature measurement and thermomechanical actuation, exhibit a high room-temperature resolution of approximately 40 mK<sup>30</sup>. While this sensitivity is somewhat inferior to that of an optimized bi-material cantilever (~ 10 mK), its active sensor area can be roughly  $10^{12}$  times smaller<sup>30</sup>. Since the thermocouple is located at the free end of the thermal probe, it benefits from better insulation from the cantilever's massive (heatsink) base, providing higher thermal resistance.

In this letter, we aim to showcase a sensitive spectroscopic technique based on the thermoelectric measurement of physisorbed molecules on a nano-thermocouple embedded within a thermal probe. The thermoelectric effect consists of two primary phenomena: the Seebeck effect and the Peltier effect. The Seebeck effect refers to the generation of a voltage difference in a material due to the presence of a temperature gradient, while the Peltier effect is the reverse process, where a voltage applied across a material creates a temperature difference. We leverage the fact that the temperature difference between the hot and cold leads plays a crucial role in driving the thermoelectric effect while the temperature profile along the lengths of the materials can be optimized for improved performance.

In our probe, two distinct metals are deposited as individual stripes on a silicon cantilever and meet near the free end of the cantilever to form a nano-junction (thermocouple). The other ends of the spatially separated metal stripes form contact electrodes on the cantilever chip's base (Fig. 1). Assuming the base remains at room temperature due to its large thermal capacitance, the thermocouple junction forms an "active window" near the tip. When the junction's temperature increases above room temperature, a voltage can be detected between the room-temperature metal electrodes on the cantilever's base.

Upon exposure to IR radiation, the nanoscale junction locally probes the heat generated by the non-radiative decay of physisorbed molecules on the tip, leading to a measurable electric potential difference. Qualitatively, we can describe the process by denoting the photothermally generated heat by  $\Delta Q$ , assuming it is contributed solely by the molecules at or near the tip thermocouple. Consequently,  $\Delta Q$  is released into a tip volume  $\Omega_{tc}$  containing the embedded thermocouple. We expect the temperature change  $\Delta T$  in  $\Omega_{tc}$  to be  $\Delta Q/mC$ , where  $m$  is the mass of  $\Omega_{tc}$  and  $C$  is its heat capacity. In response to  $\Delta T$ , a voltage difference  $\Delta V$  is induced between the reference contact electrodes at the cantilever's base, which is then amplified for readout and display. A well-insulated device with a small thermal mass can produce a large  $\Delta T$  for a small  $\Delta Q$ . Since  $\Delta Q = \Delta Q(\lambda, P)$ , where  $\lambda$  is the illumination wavelength and  $P$  is the incident IR radiation power absorbed by the molecules, the absorption spectrum of the tip adsorbates may be obtained from the thermal probe readout. We will now proceed to experimentally demonstrate the described "tip-adsorbed" photothermal spectroscopy (TAPS) and theoretically analyze the underlying mechanism.

Specifically, we computationally obtain reasonable agreement with the experiments and suggest how to optimize the design.

As shown in Fig. 1a., TAPS is implemented using a Si cantilever (length 200  $\mu\text{m}$ , width 50  $\mu\text{m}$ , and thickness 3.5  $\mu\text{m}$ ) with a 25 nm radius thermocouple embedded in its pyramidal tip. The metal leads of the thermocouple, deposited on the cantilever, are thermally insulated by a thin  $\text{SiO}_2$  layer, as explained in the Materials and Methods section. Two different methods were used to deposit the target material onto the probe: (A) via AFM imaging, wherein islands of deposited TNT on a surface are contacted by the probe; and (B) by directly populating the tip with TNT and DMMP via physical vapor deposition (PVD). Details of sample deposition are given in S1.2. Using the PVD, we also investigated polymers polydimethylsiloxane (PDMS) and polymethyl methacrylate (PMMA) owing to their unique IR absorption peaks in the spectral window considered.

The excited molecular states decay by emitting photons (radiative process) or, in the present case, predominantly by producing heat (non-radiative decay). A quantum cascade laser (QCL), tunable in  $1145 \leq \nu [\text{cm}^{-1}] \leq 1410$ , was used as the source. A calibration was carried out by measuring the TAPS signal caused by a known temperature, yielding 45 mV/K. Since the output power of the employed QCL is not constant across its spectral window (shown in Supplementary Information), our background spectral correction receives contributions from the signal with no adsorbate, as well as from the wavelength-dependent power profile of the source. To further validate the TAPS spectroscopic signal transduction, we carried out Fourier transform IR spectroscopy (FTIR) in the attenuated total reflection (ATR) configuration.

The results are shown in Fig. 1-4. The QCL output beam was amplitude modulated at 50 Hz to allow lock-in detection of the probe response (see schematics in Fig. 1c). Figure 1d shows the TAPS response when the sensor has been exposed to TNT. The TNT spectra were further explored with TAPS in Fig. 2(a) via the Method (A): AFM method, and in Fig. 2(b) via the Method (B): PVD method for comparison, and in Fig. 2(c) using the standard FTIR for validation. The observed photothermal band with a peak at 1376  $\text{cm}^{-1}$  in Fig. 2 exhibits the characteristics of  $\text{NO}_2$  stretching vibration of the TNT. We note that in these measurements, the added mass was insufficient for the mechanical resonance frequency of the cantilever (first frequency of 135 kHz with an estimated

sensitivity of 1.2 ng/kHz, see Supplementary Information) to exhibit a shift. Assuming a 1.2 ng/kHz sensitivity, a significantly higher mass than that observed in the thermoelectric measurements would be needed to detect a shift. The TAPS spectra generated using an IR laser may feature peaks that are not apparent in the FTIR spectra. Such differences are likely in part due to the different background correction procedures. In the FTIR bulk-level measurements, each acquired spectrum is corrected with that of the background (i.e., atmosphere and substrate without the specimen). In the proof-of-principle TAPS microscale measurements, to correct each spectrum, the probe must be removed, coated, and replaced. Additionally, in the TAPS setup, the QCL generates a linearly polarized beam in a single spatial mode, nominally  $\text{TEM}_{00}$  with a linewidth  $\leq 100$  MHz at FWHM when measured over 1 s with a wavelength accuracy  $\leq 1$   $\text{cm}^{-1}$ . The FTIR system employed (Bruker VERTEX 70, Massachusetts), on the other hand, achieves sample excitation using a thermal source in an interferometric configuration that generates an unpolarized beam with a spectral resolution, here, selected to be 4  $\text{cm}^{-1}$ . Furthermore, in FTIR spectroscopy, one determines the absorption of IR light by a sample (Beer-Lambert) by measuring the remaining transmitted or unabsorbed photons using photodetectors. In the TAPS technique, on the other hand, one detects IR light by the cantilever responding to the heat generated through photon absorption. As such, TAPS represents a direct and complementary calorimetric technique, in contrast to the conventional detection of photons not absorbed by the sample.

Figure 3a shows the TAPS spectrum of DMMP and its comparison with the FTIR spectrum (averaged 100 times per scan). The TAPS spectrum of PMMA is shown in Fig. 3b, while Fig. 3c shows the spectrum of PDMS. An excellent agreement is observed between the TAPS and FTIR results, demonstrating the high spectral selectivity of TAPS. The observed photothermal band with a peak at 1376  $\text{cm}^{-1}$  in Fig. 3a exhibits the characteristics of P=O stretching mode of DMMP, while the peak at 1264  $\text{cm}^{-1}$  in Fig. 3b belongs to the C–O–C stretching of PMMA. The peak at 1268  $\text{cm}^{-1}$  in Fig. 3c is assigned to  $\text{CH}_3$  deformation in  $\text{Si-CH}_3$  of PDMS. The line widths of the TAPS spectra appear broader than those observed in the FTIR measurements. In general, the broadening of the peaks in conventional solid and liquid phase IR spectra, such as seen in the FTIR spectra here, is caused by the relaxation and dephasing of the excited vibrational states and indicates the complex, fast dynamic interaction of the molecule with its environment. Clearly, in the case of TAPS spectra, other broadening mechanisms are at play, warranting further exploration.

We also note that when using the PVD-prepared cantilevers, the adsorbates located away from the tip may affect the junction temperature, given the QCL beam diameter of 2.5 mm. To support the argument that the Seebeck signal originates mainly from the thermocouple region of the cantilever, we displaced the laser beam to alter the excitation region. No thermoelectric signal could be observed when the thermocouple surface was excluded. The lack of a potential difference when exposing the cantilever surface but not the thermocouple, demonstrates that the spectroscopic signal originates mainly from the tip. The cantilever's  $\text{SiO}_2$  layer provides a barrier to the transfer of heat to the thermocouple leads. Since the (cold) reference point for the thermocouple is limited to the comparatively massive base of the cantilever, it remains at ambient temperature (here room temperature of 293 K). The mass of the cantilever is  $\sim 19$  ng while the base of the cantilever is  $\sim 75$   $\mu$ g. The experiments demonstrate that the tip is the main sensitive area, and the base of the cantilever has negligible contribution to the Seebeck voltage. These arguments are corroborated by our analysis of the computationally obtained solutions, as detailed in the below model.

To develop a model for the observed effect, we investigated the factors that could contribute to the TAPS signal. Importantly, how the photothermally generated temperature varies with the quantity of adsorbed material needs to be determined. The thermocouple temperature can be measured with a sensitivity of 0.01  $^{\circ}\text{C}$  using a low-noise electronic module (VertiSense, AppNano, California), typically used as a thermal imaging amplifier in SThM. The result, displayed in Fig. 4a, verifies the expected dependence of temperature increases with the increase in the quantity of the adsorbates. A positive correlation was also found between the TAPS signal and the laser power, as shown in Fig. 4b.

To further elucidate both the thermal and thermoelectric responses of the TAPS sensor and to illustrate how the system can be tailored for optimal performance, we conducted a computational analysis. By modeling the entire sensor system, the system's behavior can be investigated under parametric conditions. The tip is made of  $\text{SiO}_2$  and incorporates two metal substructures made of constantan and nichrome that form the two thermoelectric junctions. Obtaining the stationary thermal response of the cantilever part (sans the tip) is trivial and is not treated here as it is not critical to the thermoelectric events. Assume the sensor is made up of  $N$  layers occupying the

spatial domains  $\Omega_i, i = 1 - N$ . Prior to experiments, the sensor is at room temperature, ambient pressure of 1 Pa, and zero relative humidity so that the initial condition may be taken to be:  $T(\mathbf{x}, t)|_{t=0} = T_0 = 293.15$  K, for each sensor point  $\forall \mathbf{x} \in \Omega_i$ , prior to the arrival of the first QCL pulse. All boundaries (normal vector  $\mathbf{n}$ ), except for the tip boundary, are assumed to have zero heat flux  $\boldsymbol{\phi}$ , that is, are thermally insulated ( $\mathbf{n} \cdot \boldsymbol{\phi} = 0$ ). We assume no other sources of radiation interacts with the adsorbates. Note that the domains  $\Omega_i$  here account for all the fabrication material layers occupied by sensor domain  $\Omega$ . Given that any temperature rises above  $T_0$ , caused by the QCL pulses, follow:  $T(t)/T_0 = 1 + \delta(t)$ , where  $\delta$  is small and depends on the amplitude modulation of the QCL beam, we assume any radiative heat transfer to be negligible. Additionally, since the probe's surface area is also small, we neglect any heat transfer by convection. Preliminary computational results can readily show that the heat transport through  $\Omega$  occurs on time scales faster than ms. For the undriven cantilever subject only to noise, dissipative effects, other than the Joule heating, such as thermo-elasticity do not contribute to the temperature distribution. Therefore, for the QCL amplitude modulation frequencies considered in this work,  $f_{QCL} \sim 50$  Hz, we only need to solve the stationary ( $\partial_t T \rightarrow 0$ ) heat equation sourced by field-induced and temperature-induced (Seebeck) currents  $\mathbf{J}$  and no Peltier term:

$$\nabla \cdot [k(\mathbf{x}, T) \nabla T(\mathbf{x})] = -\mathbf{J} \cdot \mathbf{E} = -[-\sigma(\mathbf{x}, T) \nabla V(\mathbf{x}) - \sigma(\mathbf{x}, T) S(\mathbf{x}, T) \nabla T(\mathbf{x})] \cdot [-\nabla V(\mathbf{x})], \quad (1)$$

Where  $V$  is the electric scalar potential of the field  $\mathbf{E}$ , and  $\sigma, k$  are the electric and thermal conductivities, respectively, while  $S$  denotes the Seebeck coefficient of a domain. Here,  $V = 0$  is understood as the initial value of the potential, corresponding to temperature uniformity. With no other charges present, we note the current is conserved, thus:

$$\nabla \cdot \mathbf{J} = \nabla \cdot [-\sigma_\Omega(T) \nabla V - \sigma_\Omega S_\Omega \nabla T(\mathbf{x})] = 0, \quad (2)$$

where at the sensor outer boundaries, we assume no transport ( $\mathbf{n} \cdot \mathbf{J} = 0$ ). We assume  $V = 0$  V for the potential on the end boundary (terminal) of the constantan layer, while the start boundary (tip radius  $R = 25$  nm) may be modeled as an unconnected perfect conductor. Prior to presenting the

solutions, we note that using simplifying assumptions (see supplementary materials for details), the thermoelectric potential for a 1D problem may be given as:

$$\int_{V_{ref}}^V dV = \Delta V = \int_{T_{ref}}^T [S_B(T) - S_A(T)] dT. \quad (3)$$

This simple result generates a rough estimate of  $\Delta V = -60 \mu\text{V}$  (or  $60 \mu\text{V}$ ), if swapping the materials) when using  $S_B(T) \approx S_B(T_{ref}) = -35 \times 10^{-6} \text{ VK}^{-1}$  for constantan, and  $S_A(T) \approx S_A(T_{ref}) = 25 \times 10^{-6} \text{ VK}^{-1}$  for nichrome. If the IR radiation is instantly absorbed by the absorbates, which leads to  $\delta = 3.4 \times 10^{-3}$ , or a tip temperature just one degree above the initial temperature, a reasonable assumption based on the experimental observations, we obtain the temperature and thermoelectric potential distributions by solving the thermoelectric equations (see supplementary materials for details). We will first consider an overall metal electrode arrangement likely to be implemented in sensors such as that experimented with here. The results are shown in Fig. 5. For a pyramidal tip, a good estimate of the thermal response is computed in Fig. 5. These results require 3D meshing of the model tip. Since for a conical tip, only negligible deviation is expected when compared to a pyramidal tip, we also compute the conical case in which the cylindrical symmetry can be utilized to reduce the computational burden. The results are shown in Fig. 5. These results are consistent with the experimental observations and demonstrate how the design of more specialized sensors can be achieved.

In conclusion, the presented photothermal generation of spectral data by TAPS is found to facilitate robust metrology for small adsorbate quantities. The results suggest that the observed atto-gram sensitivity for molecular recognition of physisorbed molecules can be improved with additional nanofabrication optimization and design innovation including the exploration of new materials for thermal management in the neighborhood of the tip region. Given that the QCL technology could offer line widths as narrow as  $0.00002 \text{ cm}^{-1}$  or  $\sim 0.5 \text{ MHz}^{35}$ , spectral optimization can be further explored. The employed cantilever (thermal probe), fabricated to incorporate a nano-thermocouple, can therefore be viewed as a sensor platform for the detection of an exceedingly small number of adsorbates. Concluding that only the molecules adsorbed on the thermocouple tip

surface of the thermal probe produce the observed IR spectral response, is a major finding and impetus in favor of such a platform. In addition, since excitation/de-excitation times are orders of magnitude smaller than the time of temperature measurements, an extremely small number of molecules could be detected by increasing the fluence of the excitation source. Therefore, by optimizing the thermal mass, thermal conductance, irradiation time, and IR fluence, this method can provide exciting opportunities for developing high-performance sensors with very high sensitivity, selectivity, and ease of operation. The presented computational results demonstrate that design based on incorporating such material and geometry optimization strategies is possible via parametric studies of a 3D model that accurately accounts for all nanoscale material layers and shapes. For example, we envision the fabrication of an advanced tip in which a Peltier subsystem could also be integrated with the Seebeck subsystem to allow the creation of a higher temperature gradient.

## ASSOCIATED CONTENT

Additional details on the nanothermal probe, TAPS experimental arrangement, photothermal spectroscopy, the comparison of performance between the bi-material cantilever and nanothermal probe, a detailed analysis of experimental data on another set of nanoprobes, QCL power profile, calculations of adsorbed mass on the nanoprobe, and the computational model are given in the Supplementary Information. This material is available free of charge via the Internet at <http://pubs.acs.org>.

## AUTHOR INFORMATION

**Corresponding Author:** \*E-mail: [tghunda@buffalo.edu](mailto:tghunda@buffalo.edu)

**Notes:** The authors declare no competing financial interest.

## ACKNOWLEDGEMENTS

This work was supported by the School of Engineering and Applied Sciences (SEAS) University at Buffalo, The State University of New York, and NSF Award 2226614. A.P. acknowledges partial support from the Office of Biological and Environmental Research (BER) in the U.S. Department of Energy (DOE) Office of Science. The authors would like to acknowledge Drs. A. Cricic and M. Medic, the Institute of Nuclear Sciences, the University of Belgrade, for help with the physical vapor deposition setup, and Dr. A. Chand from AppNano for fruitful discussions.

## Figures:

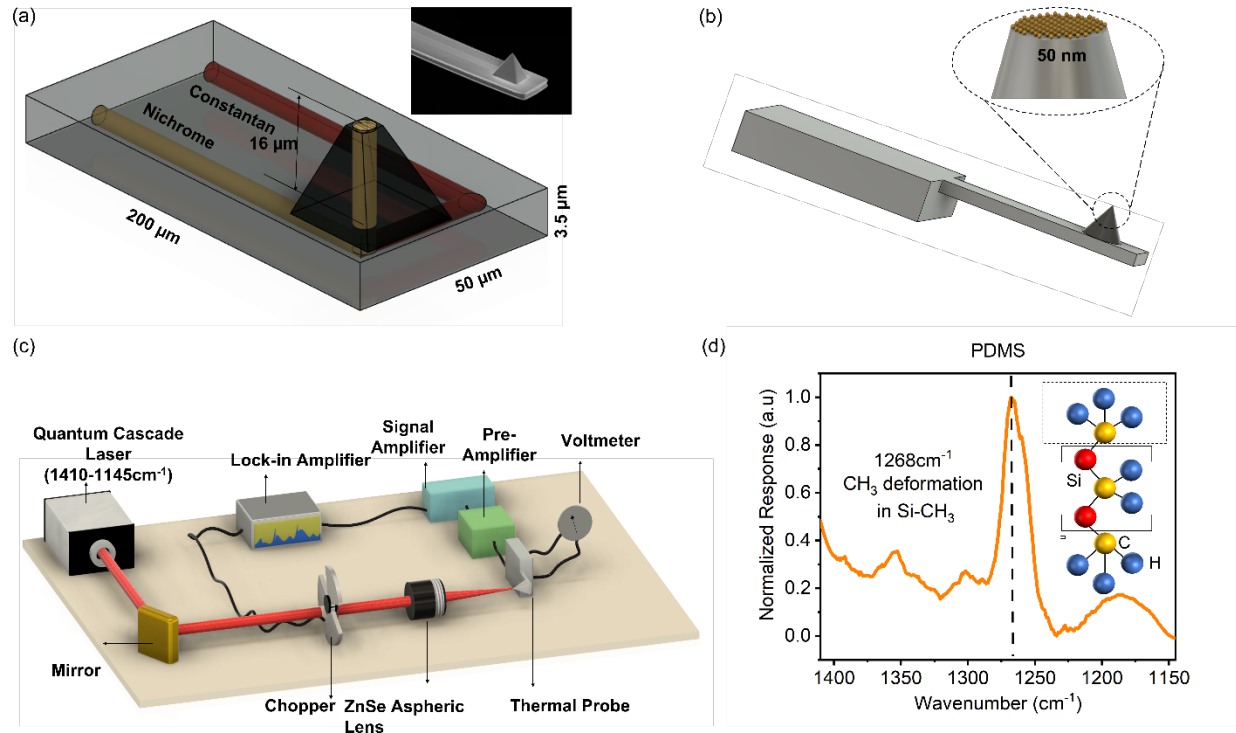


Figure 1. Tip-Adsorbed Photothermal Spectroscopy (TAPS). (a) Schematics of the embedded thermocouple on the tip of the thermal probe (image acquired with a focused ion beam during fabrication). (b) Illustration of the molecular adsorption on a 50 nm diameter tip. (c) Schematics of the experimental setup. (d) TAPS measurement of the PDMS.

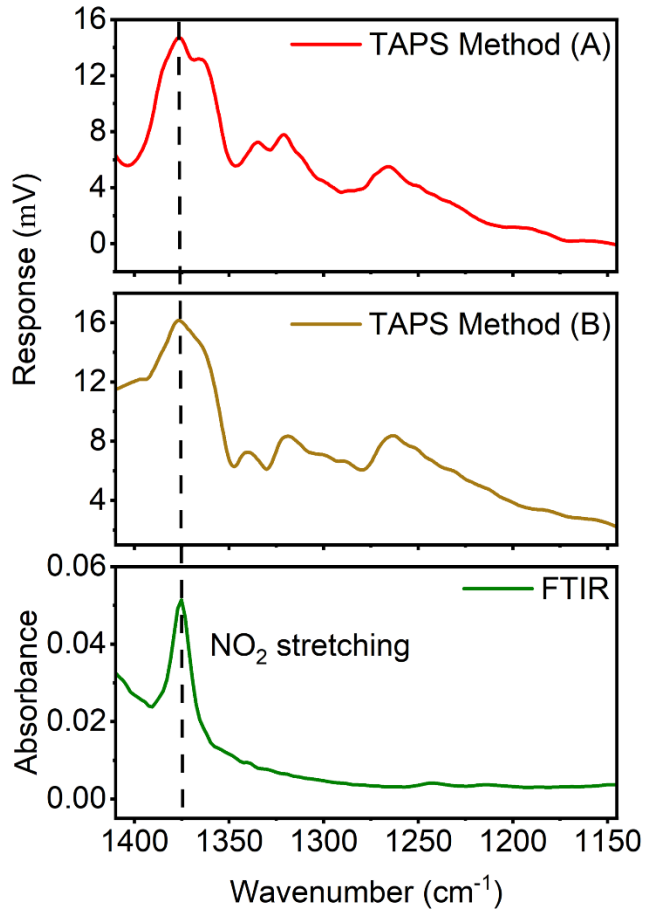


Figure 2. Comparison between TAPS and FTIR spectra of TNT. TAPS spectra exhibit additional features not observed in the FTIR spectrum. The TAPS spectra shown correspond to the two deposition methods (A) and (B), that is, AFM-image and PVD, respectively. The experimental setup amplifies the TAPS signal from  $\mu$ V to mV. (c) FTIR spectrum of TNT obtained under attenuated total reflection (ATR) condition. The single vibrational peak observed corresponds to the stretching of  $\text{NO}_2$ .

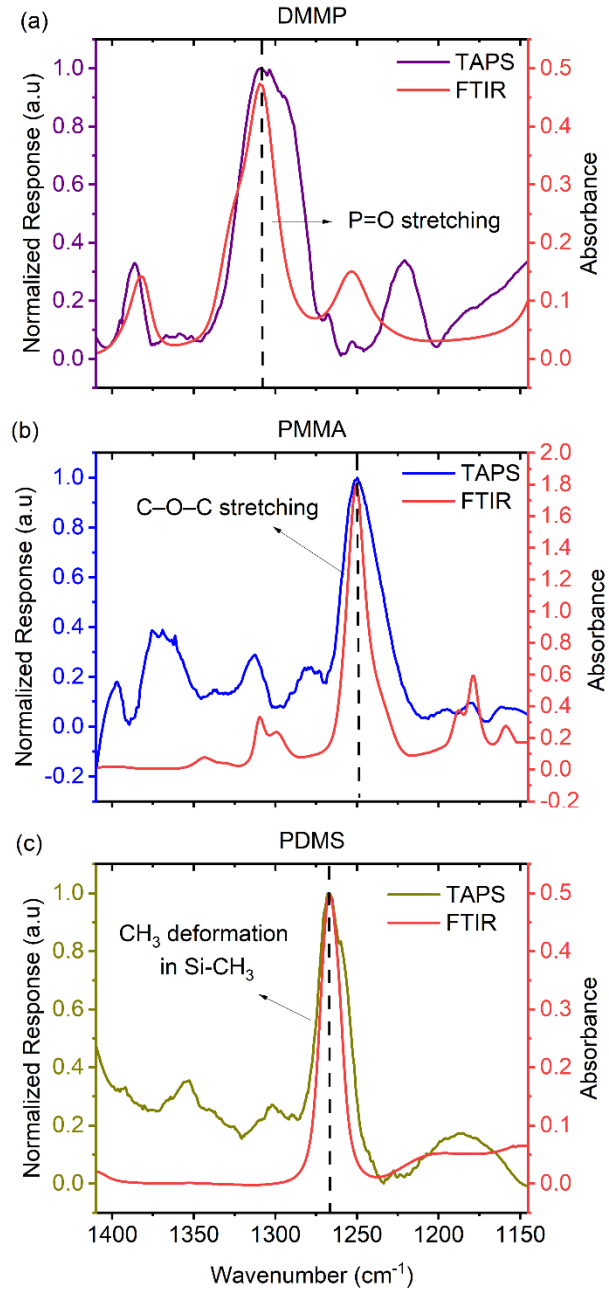


Figure 3. TAPS versus FTIR spectroscopy. (a) DMMP, (b) PMMA, (c) PDMS. All analytes were deposited via physical vapor deposition.

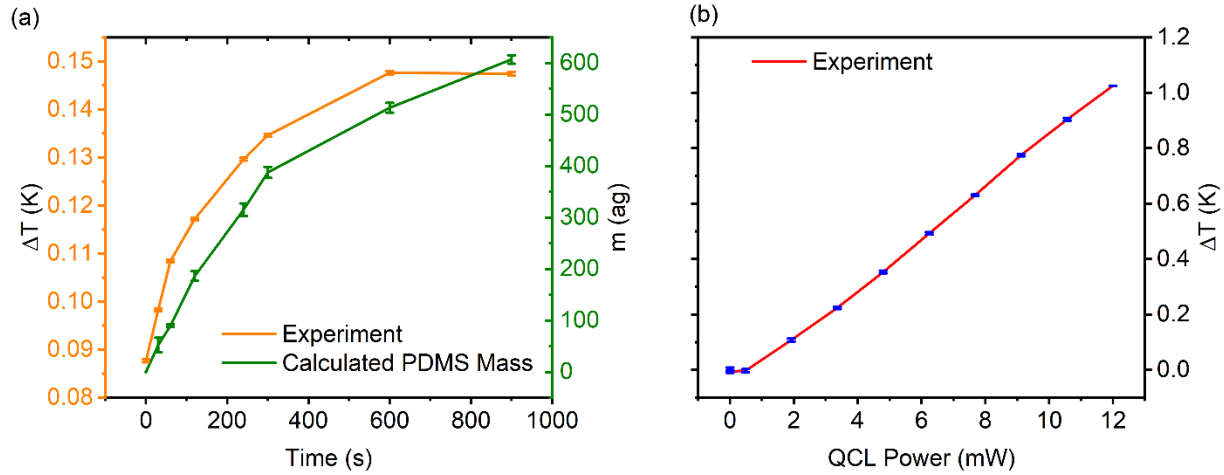


Figure 4. (a) Photothermally induced temperature changes in TAPS as a function of time and calculated adsorbed PDMS mass on the tip of the probe as a function of time. The adsorbed mass is estimated from the adsorption rate determined using a QCM in an identical setup. (b) Temperature changes in TAPS as a function of QCL output power. The experiments were conducted with a thermocouple with 384 ag of PDMS. Error bars are shown in blue.

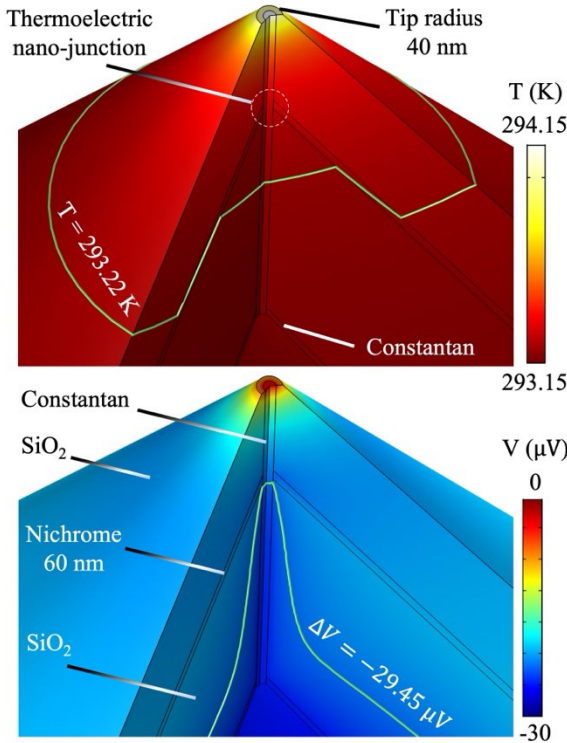


Figure 5. Computational study of the thermoelectric properties of TAPS. The temperature (top) is visualized by opening a section of the tip to display the interior distribution. The lower part of the tip and the cantilever are excluded for visual clarity. A single contour level at 293.22 K is provided to better elucidate the significant temperature discontinuity caused by the various layers. The dashed circle indicates the location of the thermoelectric junction. Owing to the nonzero Seebeck coefficients of the annotated materials, the computed temperature distribution induces an electric potential distribution (bottom). The single contour at  $-29.45 \mu\text{V}$  illustrates the behavior of the potential formed near the junction. Experimental setup amplifies the signal to mV.

## References

- (1) Murray, R. W. Chemical Sensors and Molecular Selectivity. *Anal Chem.* **1994**, *66*, A505-A505.
- (2) Strle, D.; Stefane, B.; Trifkovic, M.; Van Miden, M.; Kvasic, I.; Zupanic, E.; Musevic, I. Chemical Selectivity and Sensitivity of a 16-Channel Electronic Nose for Trace Vapour Detection. *Sensors-Basel.* **2017**, *17*, 2845.
- (3) Hsieh, M. D.; Zellers, E. T. Limits of recognition for simple vapor mixtures determined with a microsensor array. *Anal Chem.* **2004**, *76*, 1885-1895.
- (4) Desikan, R.; Armel, S.; Meyer, H. M.; Thundat, T. Effect of chain length on nanomechanics of alkanethiol self-assembly. *Nanotechnology.* **2007**, *18*, 424028.
- (5) Godin, M.; Williams, P. J.; Tabard-Cossa, V.; Laroche, O.; Beaulieu, L. Y.; Lennox, R. B.; Grutter, P. Surface stress, kinetics, and structure of alkanethiol self-assembled monolayers. *Langmuir.* **2004**, *20*, 7090-7096.
- (6) Patil, S. B.; Al-Jehani, R. M.; Etayash, H.; Turbe, V.; Jiang, K.; Bailey, J.; Al-Akkad, W.; Soudy, R.; Kaur, K.; McKendry, R. A.; et al. Modified cantilever arrays improve sensitivity and reproducibility of nanomechanical sensing in living cells. *Commun Biol.* **2018**, *1*.
- (7) Sartore, L.; Barbaglio, M.; Borgese, L.; Bontempi, E. Polymer-grafted QCM chemical sensor and application to heavy metal ions real time detection. *Sensor Actuat B-Chem.* **2011**, *155*, 538-544.
- (8) Cao, Z. X.; Yao, B. C.; Qin, C. Y.; Yang, R.; Guo, Y. H.; Zhang, Y. F.; Wu, Y.; Bi, L.; Chen, Y. F.; Xie, Z. D.; et al. Biochemical sensing in graphene-enhanced microfiber resonators with individual molecule sensitivity and selectivity. *Light-Sci Appl.* **2019**, *8*, 107.
- (9) Kummer, A. M.; Hierlemann, A.; Baltes, H. Tuning sensitivity and selectivity of complementary metal oxide semiconductor-based capacitive chemical microsensors. *Anal Chem.* **2004**, *76*, 2470-2477.
- (10) Pengfei, Q. F.; Vermesh, O.; Grecu, M.; Javey, A.; Wang, O.; Dai, H. J.; Peng, S.; Cho, K. J. Toward large arrays of multiplex functionalized carbon nanotube sensors for highly sensitive and selective molecular detection. *Nano Lett.* **2003**, *3*, 347-351.
- (11) Azizi, A.; Dogan, M.; Long, H.; Cain, J. D.; Lee, K.; Eskandari, R.; Varieschi, A.; Glazer, E. C.; Cohen, M. L.; Zettl, A. High-Performance Atomically-Thin Room-Temperature NO<sub>2</sub> Sensor. *Nano Lett.* **2020**, *20*, 6120-6127.
- (12) Hwang, Y.; Sohn, H.; Phan, A.; Yaghi, O. M.; Candler, R. N. Dielectrophoresis-Assembled Zeolitic Imidazolate Framework Nanoparticle-Coupled Resonators for Highly Sensitive and Selective Gas Detection. *Nano Lett.* **2013**, *13*, 5271-5276.
- (13) Foy, C.; Zhang, L. N.; Trusheim, M. E.; Bagnall, K. R.; Walsh, M.; Wang, E. N.; Englund, D. R. Wide-Field Magnetic Field and Temperature Imaging Using Nanoscale Quantum Sensors. *Acad Appl Mater Inter.* **2020**, *12*, 26525-26533.
- (14) Andrich, P.; Li, J. J.; Liu, X. Y.; Heremans, F. J.; Nealey, P. F.; Awschalom, D. D. Microscale-Resolution Thermal Mapping Using a Flexible Platform of Patterned Quantum Sensors. *Nano Lett.* **2018**, *18*, 4684-4690.
- (15) Gao, X. Y.; Jiang, B. Y.; Allcca, A. E. L.; Shen, K. H.; Sadi, M. A.; Solanki, A. B.; Ju, P.; Xu, Z. J.; Upadhyaya, P.; Chen, Y. P.; et al. High-Contrast Plasmonic-Enhanced Shallow Spin Defects in Hexagonal Boron Nitride for Quantum Sensing. *Nano Lett.* **2021**, *21*, 7708-7714.
- (16) Kongsuwan, N.; Xiong, X.; Bai, P.; You, J. B.; Png, C. E.; Wu, L.; Hess, O. Quantum Plasmonic Immunoassay Sensing. *Nano Lett.* **2019**, *19*, 5853-5861.

- (17) Chae, I.; Lee, D.; Kim, S.; Thundat, T. Electronic Nose for Recognition of Volatile Vapor Mixtures Using a Nanopore-Enhanced Opto-Calorimetric Spectroscopy. *Anal Chem.* **2015**, *87*, 7125-7132.
- (18) Tomic, O.; Ulmer, H.; Haugen, J. E. Standardization methods for handling instrument related signal shift in gas-sensor array measurement data. *Anal Chim Acta.* **2002**, *472*, 99-111.
- (19) Anisimov, D. S.; Chekusova, V. P.; Trul, A. A.; Abramov, A. A.; Borshchev, O. V.; Agina, E. V.; Ponomarenko, S. A. Fully integrated ultra-sensitive electronic nose based on organic field-effect transistors. *Sci Rep-Uk.* **2021**, *11*, 10683.
- (20) Krause, A. R.; Van Neste, C.; Senesac, L.; Thundat, T.; Finot, E. Trace explosive detection using photothermal deflection spectroscopy. *J Appl Phys.* **2008**, *103*, 094906.
- (21) Biswas, T. S.; Miriyala, N.; Doolin, C.; Liu, X.; Thundat, T.; Davis, J. P. Femtogram-scale photothermal spectroscopy of explosive molecules on nanostrings. *Anal Chem.* **2014**, *86*, 11368-11372.
- (22) Prashanthi, K.; Phani, A.; Thundat, T. Photothermal Electrical Resonance Spectroscopy of Physisorbed Molecules on a Nanowire Resonator. *Nano Lett.* **2015**, *15*, 5658-5663.
- (23) Itkis, M. E.; Perea, D. E.; Niyogi, S.; Rickard, S. M.; Hamon, M. A.; Zhao, B.; Haddon, R. C. Purity evaluation of as-prepared single-walled carbon nanotube soot by use of solution-phase near-IR spectroscopy. *Nano Lett.* **2003**, *3*, 309-314.
- (24) Shih, W. C.; Santos, G. M.; Zhao, F.; Zenasni, O.; Arnob, M. M. Simultaneous Chemical and Refractive Index Sensing in the 1-2.5  $\mu\text{m}$  Near-Infrared Wavelength Range on Nanoporous Gold Disks. *Nano Lett.* **2016**, *16*, 4641-4647.
- (25) Welsher, K.; Liu, Z.; Daranciang, D.; Dai, H. Selective probing and imaging of cells with single walled carbon nanotubes as near-infrared fluorescent molecules. *Nano Lett.* **2008**, *8*, 586-590.
- (26) Barnes, J. R.; Stephenson, R. J.; Welland, M. E.; Gerber, C.; Gimzewski, J. K. Photothermal Spectroscopy with Femtojoule Sensitivity Using a Micromechanical Device. *Nature.* **1994**, *372*, 79-81.
- (27) Kim, S.; Lee, D.; Thundat, T. Photothermal cantilever deflection spectroscopy. *Epj Tech Instrum.* **2014**, *1*, 7.
- (28) Bagheri, M.; Chae, I.; Lee, D.; Kim, S.; Thundat, T. Selective detection of physisorbed hydrocarbons using photothermal cantilever deflection spectroscopy. *Sensors and Actuators B: Chemical.* **2014**, *191*, 765-769.
- (29) Yamada, S.; Schmid, S.; Larsen, T.; Hansen, O.; Boisen, A. Photothermal Infrared Spectroscopy of Airborne Samples with Mechanical String Resonators. *Anal Chem.* **2013**, *85*, 10531-10535.
- (30) Shekhawat, G. S.; Ramachandran, S.; Sharahi, H. J.; Sarkar, S.; Hujasak, K.; Li, Y.; Hagglund, K.; Kim, S.; Aden, G.; Chand, A.; et al. Micromachined Chip Scale Thermal Sensor for Thermal Imaging. *Acs Nano.* **2018**, *12*, 1760-1767.
- (31) Jeremy J Goeckeritz, G. D. A., Ami Chand, Josiah F. Willard. Vertical embedded sensor and process of manufacturing thereof. USA US9389244B2 2016.
- (32) Mills, G.; Zhou, H.; Midha, A.; Donaldson, L.; Weaver, J. M. R. Scanning thermal microscopy using batch fabricated thermocouple probes. *Appl Phys Lett.* **1998**, *72*, 2900-2902.
- (33) Shi, L.; Plyasunov, S.; Bachtold, A.; McEuen, P. L.; Majumdar, A. Scanning thermal microscopy of carbon nanotubes using batch-fabricated probes. *Appl Phys Lett.* **2000**, *77*, 4295-4297.

- (34) Kim, K.; Chung, J.; Hwang, G.; Kwon, O.; Lee, J. S. Quantitative Measurement with Scanning Thermal Microscope by Preventing the Distortion Due to the Heat Transfer through the Air. *Ac<sub>s</sub> Nano*.**2011**, *5*, 8700-8709.
- (35) Ganser, H.; Frech, B.; Jentsch, A.; Mürtz, M.; Gmachl, C.; Capasso, F.; Sivco, D. L.; Baillargeon, J. N.; Hutchinson, A. L.; Cho, A. Y.; et al. Investigation of the spectral width of quantum cascade laser emission near 5.2  $\mu$ m by a heterodyne experiment. *Optics Communications*.**2001**, *197*, 127-130.